Thermochimica Acta 698 (2021) 178887

Contents lists available at ScienceDirect

Thermochimica Acta

journal homepage: www.elsevier.com/locate/tca

A DSC signal for studying kinetics of moisture evaporation from lignocellulosic fuels

Alexander N. Kozlov [a,*], Vitaly A. Shamansky [a], Igor G. Donskoy [a], Maxim V. Penzik [a], Alexandre V. Keiko [b]

[a] Melentiev Energy Systems Institute SB RAS, 130 Lermontov Str., Irkutsk, 664033, Russia
[b] Energy Research Institute of Russian Academy of Sciences, 31 Nagornaya Str., Moscow, 117186, Russia

ARTICLE INFO

Keywords:
Wood biomass
DSC signal
Water adsorption energy
Kinetics of drying

ABSTRACT

The study of the pine sawdust drying kinetics was carried out using thermal analysis. The evaporation rate of free and bound moisture was determined using thermogravimetric data. Differential scanning calorimetry allows to evaluate the effect of evaporation on the deviation of the sample temperature from the heating gas temperature. In experiments, this temperature deviation increases with the heating rate and can be several tens of degrees. Using the developed theoretical approach, the values of the energy of moisture sorption were obtained from the data on the rate of evaporation at different temperatures under conditions of diffusional evaporation (the period of decreasing drying rate). This approach operates with the thermodynamic parameters of interfacial interaction, which affect the change in the saturated pressure of water vapor above the biomass surface. The results show that with a decrease in the moisture content of the pine wood, the sorption energy of moisture increases rather sharply, and at a moisture content of less than 5%, this dependence is close to exponential.

1. Introduction

Wood biomass is an attractive energy resource due to its availability, renewability and environmental friendliness (compared to coal and hydrocarbons). There is a wide range of technologies for biomass conversion into energy: combustion, pyrolysis, gasification, bioprocessing, etc.

Wood is a complex composite consisting of macromolecules of different types, that has specific structural characteristics. The properties and composition of wood vary widely depending on the sort and history of a sample. These features determine the complexity of transfer phenomena in wood (diffusion, thermal conductivity, filtration). In turn, these phenomena determine many practically important processes, first of all, drying, which can be both a target stage when wood is used as an engineering material, and an intermediate stage during its thermal processing. In the latter case, the wood is often exposed to intense thermal effect. In such conditions, the widely used simplified models of the drying process become inadequate.

According to the classification proposed by A.V. Lykov [1], wood is a capillary-porous body. In addition to the system of large pores, there is a developed system of capillaries in the wood that are less than a micrometer in size [2–4]. Pores provide permeability of wood for condensed moisture and water vapor, as well as excessive vapor-pressure equilibrium. This is why their size largely determines the kinetics of drying. Humidification and drying of wood are accompanied by changes in linear dimensions and porous structure, therefore effective transfer coefficients are often very sensitive to moisture content of a sample [5,6]. Moisture in wood is in several states [7]. Usually, for simplicity, two

Abbreviations: DSC, differential scanning calorimetry; STA, synchronous thermal analysis; TG, thermogravimetry; *a*, empiric coefficient; *b*, empiric coefficient; *D*, diffusivity, m^2/s; *Eads*, adsorption energy, J/mol; *h*, specific enthalpy, J/mol; *IDSC*, DSC signal, W; *Jw*, evaporation rate, kg/s; *jdr*, drying rate, $kg/m^2/s$; *Kev*, evaporation rate coefficient, $kg/m^2/s/Pa$; *Kr*, pseudo-kinetic coefficient, 1/s; *kD*, transfer number, kg/s/Pa; *lev*, specific evaporation heat, J/mol Nu – Nusselt number; *m*, sample mass, kg; *P*, pressure, Pa; Pr, Prandtl number; *pw*, saturated vapour pressure, Pa; *Qev*, evaporation heat, J/kg; *q*, heat flux, W; *R*, universal gas constant, J/mol/K; Re, Reynolds number; *r*, crucible radius, m; *S*, surface area, m^2; *Ssp*, specific wood internal surface, m^2/g; *s*, specific enthropy, J/mol/K; *T*, temperature, K; *t*, time, s; *tend*, evaporation time, s; *x*, spatial coordinate, m; *W*, water content, kg/kg; *w*, moisture fraction, %; α, heat transfer coefficient, $W/m^2/K$; β, mass transfer coefficient, $kg/m^2/s/Pa$; δ*w*, water height in crucible, m; δ*D*, diffusion layer thickness, m; δ*w*, sorption layer thickness, m; λ, thermal conductivity, W/m/K; μ, chemical potential, J/mol; ρ*w*, water density, g/m^3.

* Corresponding author.
E-mail address: kozlov@isem.irk.ru (A.N. Kozlov).

https://doi.org/10.1016/j.tca.2021.178887
Received 16 May 2020; Received in revised form 23 January 2021; Accepted 27 January 2021
Available online 1 February 2021

types of moisture are distinguished: free and bound moisture but sometimes additional gradations are identified. These states of moisture differ in the energy required for its evaporation. In this case, evaporation is represented as a sequence of phase transitions between moisture of different types until the final transformation into vapor occurs.

The processes of drying and thermal decomposition can overlap [8,9] during pyrolysis and combustion of wood particles (in furnaces, pyrolyzers, gasifiers). This results in changes in the porous structure of the char and in the kinetics of its gasification [10–13], in the conditions for combustion of a solid fuel in fixed bed and of pyrogas above wood surface [14–17]. This also leads to the formation of Stefan flow that affects the rate of heterogeneous reactions and aerodynamics of particles [18]. In the case of a very rapid heating (for example, due to intense radiation) there can be a steam explosion leading to the particle destruction [19]. High initial moisture of a fuel under intensive heating produces steam that acts as a gasification agent [20–22]

Kinetics of drying is experimentally studied for both individual particles and backfilling. One of the widely used methods is thermal analysis, including thermogravimetric analysis [23–25] in combination with differential scanning calorimetry (DSC) [26–28].

A thermal diffusion model of moisture transfer was proposed by A.V. Lykov [1,29]. In this model, consideration is given to thermal conductivity, diffusion and thermal diffusion of moisture, and the rate of phase transitions is averaged over an elementary volume. In this case, the effective transfer coefficients, however, often prove to be purely empirical values that are very sensitive to experimental conditions. Simplifying the Lykov model, we can obtain a diffusion model [30,31]. In the studies discussed in [32–35], the authors use numerical and analytical approaches to solve the system of Lykov equations (in a full form and a truncated form). More detailed models are based on the theory of multiphase media and include the filtration transfer equations [36–38]. In these cases, the drying rate of the particles is determined through the diffusion and convective flow of moisture of different types at the interphase boundary.

In [39], the study identifies three states of water in a wood particle: vapor, liquid film, and sorption moisture. Transfer coefficients and heat of evaporation were estimated for all states of moisture. The transition from one state of moisture to another was determined through the boundary values of local moisture. In [40], the authors proposed three types of moisture in wood: capillary, bounded and vaporous. The calculations showed that, at low heating rates, the main contribution to moisture transfer is made by bound and capillary moisture, whereas at high rates – by water vapor. Three types of moisture were also considered in the models presented in [38,41].

Much more often, the modeling of thermal conversion processes involves simplified approaches, including widely applied balance estimates [42], identification of the evaporation front and solving the corresponding Stefan problem [43,8,44–48]. At low rates of interphase heat and mass transfer, the process can be described more simply in terms of the effective transfer coefficient [49–54]. At high intensity of interphase transfer, an effective moisture diffusion coefficient can be introduced [24,55–57]. In the studies discussed in [58–60,25], the authors use the effective drying rate coefficient that normally has an Arrhenius temperature dependence, which follows from the kinetic theory of evaporation [61]. This kinetic coefficient is often associated with the diffusion coefficient, but the form of the kinetic equation for drying is similar to that for the one-stage pseudo-chemical reaction:

$$\text{Wood } (H_2O) => \text{Wood} + H_2O$$

The rate of the phase transition at the evaporation front is modelled in a similar way [62,63]. In [27,64,65] the authors approximate the drying curves with suitable functions (devoid however of a clear physical meaning). Such data can be used either in a graphical form or in a tabular form but the applicability of this approach is very limited.

In this paper, given the adsorption interaction, we propose a kinetic model of moisture evaporation from wood. This model relies on the basic concepts of interphase equilibrium (it is based on the model No. 2 in Table 1). The parameters for this model are determined using thermal analysis. A simple experimental scheme is proposed that allows to determine the sorption energy and its dependence on moisture.

2. Experimental section

In this work, two types of experiments were carried out: evaporation of free water and evaporation of moisture from wet wood. The experiments were carried out on an STA 499 F1 thermal analysis equipment. Distilled water was used for both types of experiments. The use of two types of experiments is associated with the need to calibrate the DSC signal: when processing data on sawdust drying, the characteristics associated with the thermal inertia of the device are used.

Experiments of the first type were carried out as follows. Distilled water was poured into a corundum cylindrical crucible (diameter - 5 mm, height - 5 mm, water sample mass is 80−100 mg). Weight loss was measured under linear increase in the temperature on the crucible surface. The crucible was purged with absolutely dry argon (90 ml/min). Simultaneously, the DSC signal was recorded. Water evaporation was carried out both at a constant temperature (50, 70, and 90 °C) and at a constant heating rate (1, 5, and 30 K/min up to 200 °C).

Experiments of the second type were carried out with pine sawdust soaked in water (the water:sawdust ratio is approximately 4:1, the exposure time is 24 h for complete saturation). Pine sawdust was presieved through a caliber of 0.06−0.12 mm. Externally, the sample had the form of a wet spongy mass without a visible phase of liquid water. The weight of the sample of wet sawdust in experiments is 50−70 mg. Drying of wood was carried out at a constant temperature below the temperature of the onset of thermal decomposition (50, 70 and 90 °C).

3. Theoretical section

3.1. DSC data processing

When the crucible is heated with water, evaporative cooling occurs, as a result of which the temperature of the sample can be significantly lower than the ambient temperature. In order to assess this effect, it is necessary to study the DSC signal.

During the experiment, a heating gas (argon) flows around the crucible with the sample, water evaporates and water vapor diffuses into the flow (Fig. 1). The crucible wall is thin enough that its thermal resistance can be neglected. According to the theory [75], the DSC signal value is proportional to temperature difference between reference sample and reacting sample. The difference is related to the thermal effects of processes taking place in the sample within crucible and is proportional to intensity of internal heat source (or sink). In our case, these are the processes of heating and evaporation of moisture, i.e.:

$$bI_{DSC} = q^h + q^{ev} \tag{1}$$

where I_{DSC} – DSC signal; q^h – heat for the moisture heating; q^{ev} – heat for evaporation; and b is an empirical coefficient, representing thermal inertia of crucible. Further, we assume that the sample in the crucible can be characterized by an average temperature (estimates show that the Biot number under the indicated conditions is about 10^{-3}–10^{-2}, which means that the temperature distribution in the sample is sufficiently uniform). This average temperature may differ from the ambient temperature due to evaporative cooling. If we assume that most of the heat goes to evaporation of moisture, we can write the relationship as follows:

$$bI_{DSC} \approx q^{ev} = \frac{\lambda_w S}{\delta_w}(T - T_S) \tag{2}$$

or:

Table 1
Models of wood drying and their formulas.

No.	Limiting stage	Expression of drying rate	Coefficient	Notes	References
1	External heat transfer	$j_{dr} = \frac{\alpha(T_{env} - T)}{Q^{ev}}$	$\alpha = f_1(\mathrm{Re}, \mathrm{Pr})$	Temperature distribution in a particle is considered to be uniform	[66]
2	External mass transfer	$j_{dr} = \beta\left(P^{eq}_{H_2O} - P_{H_2O}\right)$	$\beta = f_2(\mathrm{Re}, \mathrm{Pr})$	Moisture distribution in a particle is considered to be uniform	[67,68]
3	Internal heat transfer	$j_{dr} = \frac{1}{Q^{ev}}\left(\lambda\frac{\partial T}{\partial x}\right)_{x=F}$	$\lambda = f_3(W, T)$	Temperature gradient is taken at the boundary of evaporation front (Stefan problem)	[69,70]
4	Internal mass transfer	$j_{dr} = \left(D\frac{\partial W}{\partial x}\right)_{x=F}$	$D = f_4(W, T) = = D_0(W)\exp\left(-\frac{E_1}{RT}\right)$	Temperature gradient is taken at the boundary of evaporation front (normally at the external surface)	[71,72]
5	Phase transition rate	$j_{dr} = K_{evap}(p^w - p^{st})_{x=F}$	$K_{evap} = f_5(P, T) = = A(P, T)\exp\left(-\frac{E_2}{RT}\right)$	K_{evap} is a rate of phase transition known from kinetic theory; equilibrium pressure allows for the correction of capillary effects	[73]
6	Rate of pseudochemical reaction	$j_{dr} = K_r W$	$K_r = k_0\exp\left(-\frac{E_3}{RT}\right)$	The model is equivalent to the diffusion one (No. 4)	[74]

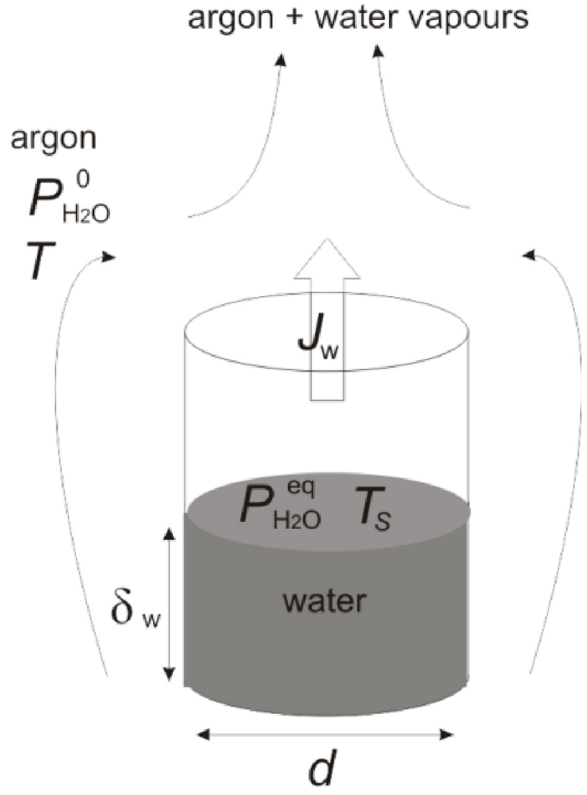

Fig. 1. Simplified scheme of water evaporation in TG experiments.

$$T_S \approx T - \frac{bI_{DSC}\delta_w}{\lambda_w S} = T - \frac{bI_{DSC}\delta_w}{\lambda_w \pi d\left(\delta_w + \frac{d}{4}\right)} \quad (3)$$

Here T_S – the temperature of evaporation surface, T – the measured temperature of the crucible surface, λ_w – теплопроводность образца, S – the surface of water and crucible contact, δ_w – the evaporating water height calculated using the thermal analysis data ($\delta_w = m_w/(\rho_w)$, where m_w – water mass in crucible, ρ_w – water density), d – inner diameter of the crucible. Thus, it is possible to clarify the temperature of the samples during the evaporation of water and drying of wood under the conditions of a thermal analysis device.

3.2. Moisture sorption energy and diffusional effects

Moisture is present in the wood pulp in different energy states. However, regardless of the diversity of such states, the process of moisture evaporation into the environment runs only through the external surface of the particle. The sum of cross-sections of the external orifices of the capillaries should be considered as such a surface. It can be assumed that the various states of moisture inside the particle are in mutual equilibrium, which is established faster than the equilibrium between the particle and the environment. Under isothermal conditions, the water molecules along the capillary walls are transported along the isoenergy surface up to the external boundaries, where a partial pressure gradient that determines the evaporation rate is formed. In equilibrium, the partial pressures of moisture inside and outside the wood level off. In this case, chemical potentials of gaseous and condensed moisture are also equal, i.e.: $\mu_{liq} = \mu_{gas}$, or:

$$\mu^0_{liq} - \varepsilon_{ads} = \mu^0_{gas} + RT\ln\left(p_{eq}/P\right) \quad (4)$$

where μ^0_{liq} and μ^0_{gas} – the standard chemical potentials of liquid water and vapor, J/mol; ε_{ads} – additional heat of water evaporation due to the interaction with the wood surface, J/mol [76]; p_{eq} – the saturated vapor pressure, Pa; P – the total pressure in the system, Pa. Since the energy state of the liquid surface inside the capillaries depends on the layer thickness and consequently on the total moisture of the wood, the value of E_{ads} can be estimated from an analysis of relationships between the saturated vapor pressure and temperature at constant moisture. This circumstance also applies to a partially filled capillary, since there is an equilibrium between the surface of the meniscus and the surface of moisture adsorbed on the walls of a capillary in contact with it. To this end, (4) will be represented as follows, considering that $\mu^0 = h^0 - Ts^0$:

$$R\ln(p_w/P) = s^0_{gas} - s^0_{liq} + \frac{h^0_{liq} - h^0_{gas} - \varepsilon_{ads}}{T} = \Delta s^0 - \frac{\varepsilon_{ads} + l_{ev}}{T} \quad (5)$$

where l_{ev} – heat of free water evaporation, J/mol; s – specific enthropy, J/mol/K; h – specific enthalpy, J/mol.

Switching to the model of kinetics of water evaporation from wood particles, it is worth noting that the impact of adsorption on the evaporation process implies primarily a change in the energy of water molecules in the condensed phase due to its interaction with the surface of wood capillaries.

The process of liquid evaporation can be considered as a conditional reversible endothermic chemical reaction, where a molecule, bypassing some potential barrier, transitions from one energy state to another. The presence of a surface layer at the interphase boundary characterizes the staged nature of such a transition, which, in terms of chemical kinetics, represents a set of consecutive chemical reactions with successive build-up of the potential barrier between the initial liquid and final gaseous state. At the phase boundary, there is a surface layer due to intermediate transition states between the initial liquid and final gaseous states, i.e. the total evaporation process approximates the sequence of transitions between such states. Thus, according to a simplified consideration, the evaporation process consists of two successive transitions: of the flow of

molecules from the liquid volume to the surface layer and their diffusion transfer from the surface layer to the gas phase. In this case, the diffusion flow is limiting, therefore an equilibrium is established between the liquid phase and the surface layer, and it is determined by the relationship $\mu_{liq} = \mu_{gas}$. Moreover, the concentration of water vapor at the outer boundary of this layer will correspond to the pressure of saturated vapor at a given temperature, i.e. the temperature of water surface. It is worthwhile to note that the vapor pressure under these conditions corresponds to the concentration of free water molecules, which are in equilibrium with various associates (groups of molecules that retain some of the hydrogen bonds characteristic of the condensed phase) in the surface layer. The limiting diffusion flux can be found from the standard diffusion equation, given the experimental conditions. Для установившегося потока газа вокруг тигля МоЖно рассМатривать процесс диффузии в приблиЖении приведенной пленки:

$$J_w = \frac{D_w S M_w}{\delta_D RT}\left(p_{eq} - p_w\right) = k_D(T)\left(p_{eq} - p_w\right) \quad (6)$$

where J_w – evaporation rate, kg/s; S – evaporation surface area, m^2; D_w – diffusion coefficient, m^2/s; M_w – Молярная Масса воды, кг/Моль; p_{eq} – the pressure of saturated vapor at a given temperature, the pressure is determined from relationship (1) at $\varepsilon_{ads} = 0$; p_w – pressure of water vapor in a gas phase, Pa; δ_D – apparent thickness of the diffusion layer, m. The thickness of the diffusion layer depends on the flow parameters. When a cylindrical body is flowed around, the diffusion layer thickness at its edge may be determined by the relation [77]: $\delta_D = d/\mathrm{Nu}$; $\mathrm{Nu} = 0.5\mathrm{Re}^{0.5}\mathrm{Pr}^{0.38}$.

Since the sample in the system was purged by the absolutely dry argon (no more than 0.0003 % of vapor), the value of p_w in equality (3) may be taken equal to zero, and considering that the saturated vapor pressure in accordance with (1) may be expressed: $p_{eq} = P\exp\left(\frac{\mu^0_{liq} - \mu^0_{gas}}{RT}\right)$, we will write (6) as:

$$J_w = \frac{D_w S M_w P}{\delta_D RT}\exp\left(\frac{\mu^0_{liq} - \mu^0_{gas}}{RT}\right) = k_D(T)\exp\left(\frac{\mu^0_{liq} - \mu^0_{gas}}{RT}\right) \quad (7)$$

The binary diffusion coefficient is proportional to a one-and-a half temperature degree [78]: $D_w \sim T^{3/2}$. This magnitude has a weak dependence on the temperature, therefore, preexponential factor in (7) can be written as $k_D(T) = k^0{}_D T^{1/2}$. Based on (2), the obtained expression may be transformed into the form:

$$J_w = k^0_D\sqrt{T}exp\left(\frac{\Delta s^0}{R}\right)\exp\left(-\frac{l_{ev}}{RT}\right) \quad (8)$$

or considering that Δs^0 in the studied temperature range weakly depends on the temperature we have:

$$R\ln\left(J_w\Big/\sqrt{T}\right) = R\ln\left(\bar{k}^0_D\right) - \frac{l_{ev}}{T} \quad (9)$$

On the basis of this fact and subject to (4) and (5), for the case of moisture evaporation from the wood surface relation (8) may be written in the form:

$$J_w = k^0_D\sqrt{T}exp\left(\frac{\Delta s^0}{R}\right)\exp\left(-\frac{l_{ev} + \varepsilon_{ads}}{RT}\right) = \bar{k}^0_D\sqrt{T}\exp\left(-\frac{l_{ev}}{RT}\right)\exp\left(-\frac{\varepsilon_{ads}}{RT}\right) \quad (10)$$

where ε_{ads} may depend on wood moisture. Under the isothermal conditions:

$$J_w = \bar{k}^0_D(T)\sqrt{T}\exp\left(-\frac{l_{ev}}{RT}\right)\exp\left(-\frac{\varepsilon_{ads}}{RT}\right) = J^0_w\exp\left(-\frac{\varepsilon_{ads}}{RT}\right) \quad (11)$$

hence:

$$\varepsilon_{ads} = -RT\ln\left(J_w/J^0_w\right) \quad (12)$$

In other words, if the adsorption energy ε_{ads} is a decreasing function of humidity, then at high humidity values, free moisture evaporates, with $\varepsilon_{ads} = 0$ and $J_w = J^0_w$. With decreasing humidity, ε_{ads} increases, which means that the evaporation rate J_w becomes lower. From this decrease in the evaporation rate, the sorption energy ε_{ads} can be determined using Eq. (12).

4. Results

4.1. Water evaporation

Fig. 2 shows TG-curves of free water evaporation. The heating rate determines the heat transfer conditions in the crucible, so the curves are expectedly different. As can be seen from the graphs, the temperature of the external surface of the crucible in the case of heating rates of 5 and 30 K/min significantly exceeds the boiling point of water, although the boiling itself is not observed, since this process would certainly affect the monotony of the curves. As mentioned above, the temperature of the water inside the crucible is lower than heating gas temperature due to the evaporation cooling and differs from the temperature recorded by the device. Moreover, it is obvious that the temperature of the liquid water phase is non-uniform and varies from the surface of contact with crucible to the evaporation surface, where the endothermic process takes place.

In order to specify the real conditions of the evaporation process, DSC signal processing technique was used. DSC curves are presented in Fig. 3. In accordance with the operation principles of the thermal analysis system, the temperature change program is performed on the basis of a signal from the surface of the crucible with the sample. In this case, if endothermic processes occur in the crucible, the temperature of the external heat carrier rises to compensate them. Inertia of this process can be seen from the curve of evaporation at a heating rate of 30 K/min (Fig. 3), when the moisture has evaporated but the process of "thermal pumping" still continues and the temperature exceeds a given limit for some time. Its subsequent decline to the norm leads to a curve deviation to the left.

The time dependences of the heating gas temperature during the experiment are shown in Fig. 4. These dependences show that the temperature program of the experiment at high heating rates is not maintained accurately enough. The device automatically compensates for the temperature difference between the crucible and the heating gas, therefore, with rapid evaporation and intense heat absorption, the heating gas temperature can exceed 473 K. At a heating rate of 5 K/min, a small step of about 7 K is observed in the area of the maximum

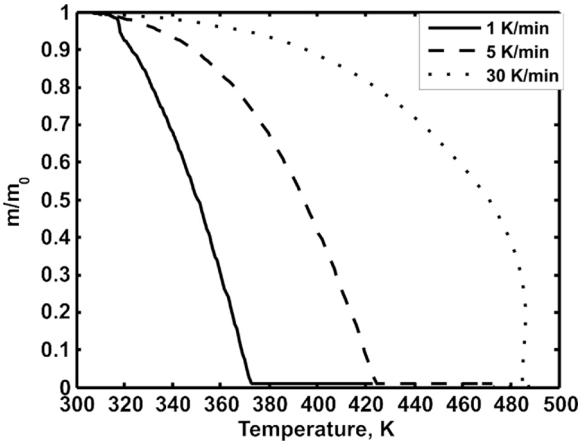

Fig. 2. Water evaporation curves. Heating rates (from left to right), K/min: 1, 5, 30.

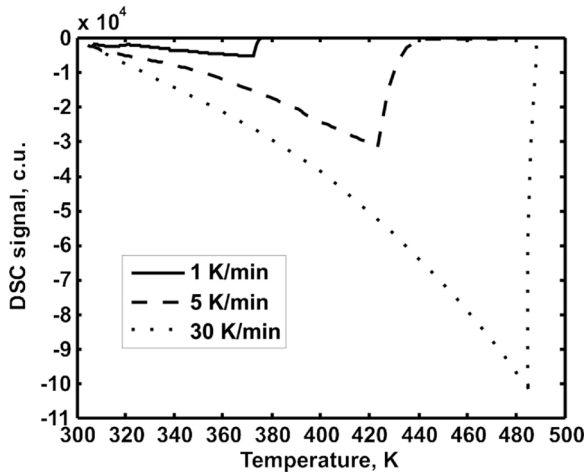

Fig. 3. DSC signal (relative current units, c.u.) in the process of water evaporation. Heating rates (top to bottom), K/min: 1, 5, 30.

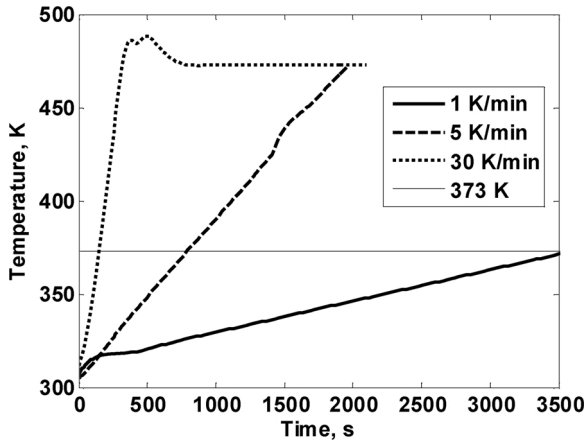

Fig. 4. Temperature curves during water evaporation experiments. Heating rates (from right to left): 1, 5, and 30 K/min. Thin solid line is level of boiling temperature.

evaporation rate. Evaporation occurs at 30 K/min so intensively that overheating reaches 15 K. The recovery time of the temperature program (transition to isothermal holding) is about 5 min.

The results of the calculation based on (3) are shown in Fig. 5. For convenience, the time scale (x-axis) in Fig. 5 is given in relative values, t/t_{end}, where t_{end} is complete water evaporation time in each experiment. At a heating rate of 1 K/min, the time of complete evaporation t_{end} is 2880s, at a heating rate of 5 K/min t_{end} = 1275s, and at a heating rate of 30 K/min, t_{end} = 300 s. As can be seen from the Fig. 5, the actual temperature of the evaporation surface differs significantly from that recorded by the TGA system in all cases.

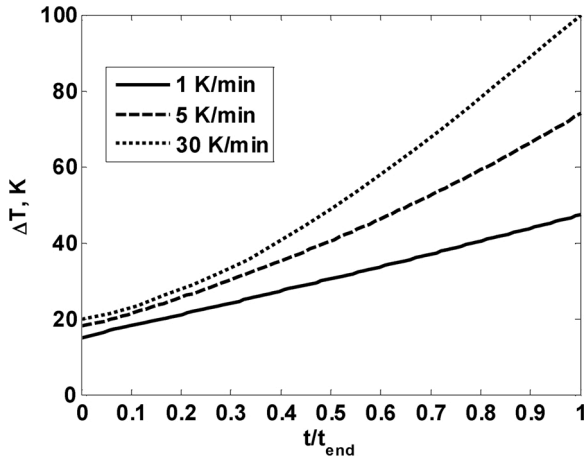

Fig. 5. Temperature deviations $\Delta T = T–T_S$ (3) calculated from the TGA data for different heating rates.

To determine the heat of vaporization of water, Eqs. (9) and (10) are used. Fig. 6 presents dependence of $F_w = R\ln(J_w T^{-1/2})$ on the reciprocal evaporation surface temperature which is calculated by (3). The evaporation rate was calculated on the basis of the thermogravimetric curves (Fig. 2) as a finite difference derivative of the sample mass with respect to time: $J_w = \Delta m/\Delta t$.

The Fig. 6 shows that relation (9) is linear for all studied heating rates. The values of l_{ev} determined from the tangent of curve slope are 44.04, 43.58 and 44.68 kJ/mole in accordance with the increasing heating rates.

Evaporation of free water without significantly influencing evaporative cooling was considered under constant temperature conditions. Fig. 7 presents experimental values of water evaporation and calculated values (solid lines) by Eq. (11). Applying Eq. (9), we can also estimate the value l_{ev}: it is equal to 44.39, 44.24 and 44.15 at 50, 70 and 90 °C, respectively, which indicates a fairly good agreement with the values obtained at constant heating rate. The values of k_D^0 are 2.95, 2.76 and 3.16; the average one is 2.96.

As is seen from the Fig. 7, the calculated and experimental values coincide fairly well, which allows the conclusion on adequacy of the postulated model representations. Minor deviations of the experimental values from the calculated ones towards the process completion is related with small variations of evaporation surface temperature.

4.2. Pine sawdust drying

TG-curves of pine sawdust drying at temperatures of 50, 70, and 90 °C are shown in Fig. 8. The initial sections of the curves are not isothermal, since at this time interval the predetermined temperature was adjusted in the furnace. The curve sections corresponding to the process of isothermal evaporation which is limited by the surface diffusion (recalculated for a new initial state) are presented in Fig. 9.

The initial linear sections that allow us to determine k_D are well seen on these curves. It is necessary to underline the following fact. In relation (7) it is supposed that the evaporation area does not change during drying. When we deal with an individual wood particle, it seems to be so, since the evaporation proceeds through the external capillary orifices, which change negligibly during drying. In addition, the diffusion of particles from the wood surface is the limiting factor, and the vapor pressure in capillary channels will be saturated for the given level of

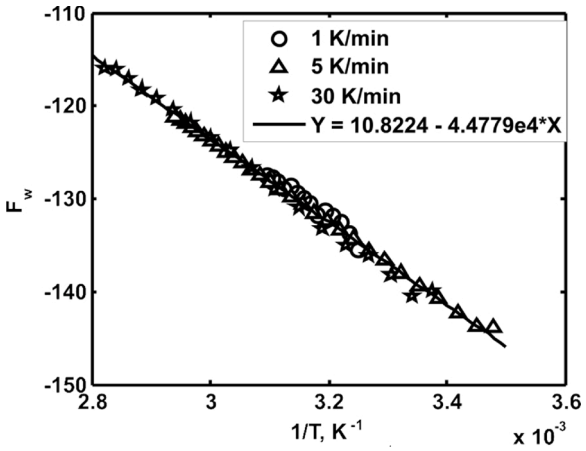

Fig. 6. The experimental values of $F_w = R\ln(J_w/\sqrt{T})$ versus $1/T$ (see Eq. (9)).

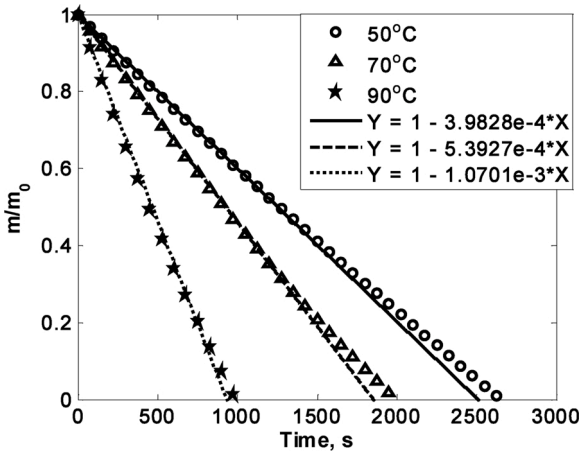

Fig. 7. Experimental and calculated (solid lines) TG curves of water evaporation at constant temperature conditions.

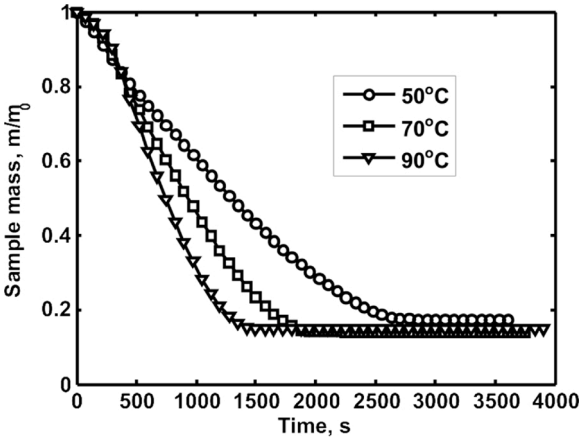

Fig. 8. Experimental curves of water-saturated sawdust drying.

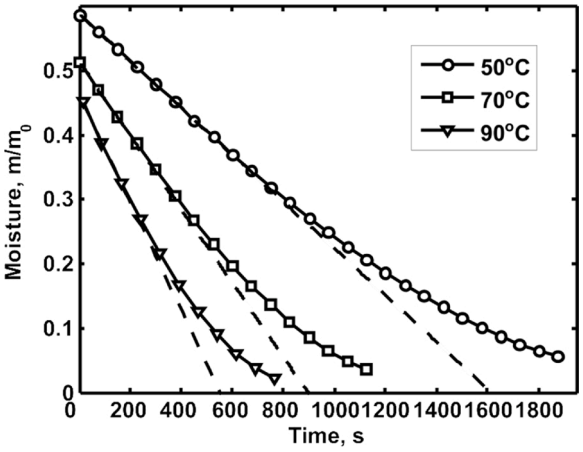

Fig. 9. Curve sections of the isothermal water evaporation from water-saturated sawdust surface.

wood particle moisture (at high temperature gradients the gas-dynamic flows can also emerge near the surface). This condition is obviously not satisfied in the case of "external" capillaries emerging during formation of hydrophile particles of different sizes. However, it may be assumed that since such capillaries cannot be long, the change in the external surface during drying will have a minor effect on the calculation results in this case. Availability of rather obvious linear initial sections indirectly confirms such a supposition. The results of calculation by equality (12) are presented in Fig. 10.

The Fig. 10 shows that at different temperatures in the region of equal moisture the curves coincide well enough. Divergence in the curves in the region of low moisture is apparently indicative of the change in the mechanism of moisture evaporation from the diffusion kinetics to the chemical one, when other regularities are in force. Thus, the kinetics of pine sawdust drying can be described using Eq. (6), in which the change in the evaporation heat is corrected with respect to ε_{ads} (4). Most importantly, the ε_{ads} value can be specified as a continuous function of moisture, which makes it possible to improve drying models compared to the approach when moisture is transformed into different forms stepwise. This approach can be naturally incorporated into complex physicochemical models of drying and thermochemical conversion of wood particles.

If we assume that the inner surface of the wood is uniformly filled with water, then the thickness of the sorbed water layer can be estimated. The relation between the moisture and sorption layer thickness δ_s is determined by the equation $\delta_s = W/(S_{sp}\rho_w)$, where S_{sp} – the specific wood surface, m^2/g; ρ_w – the water density, g/m^3; W – moisture content, g/g (the value of W is related to the humidity w by a simple relation $W = 100w/(100\text{-}w)$). If the specific surface area is assumed to be equal to 100 m^2/g [79,80], then $\delta_s = 10W$ nm. Dependence of $\ln(\varepsilon_{ads})$ on δ_s for the curve obtained at 90 °C is presented in Fig. 11.

The Fig. 11 shows that this dependence may be assumed linear, then the relation $\varepsilon_{ads} = \varepsilon^{\circ}\exp(-a\delta_s)$ is satisfied that may be associated with influence of the long-range forces [81]. The orientation Coulomb interaction of the polar water molecules with the charged wood surface sections (adsorption centers) with formation of a polymolecular adsorption layer takes apparently place in this case. The water molecules are oriented layer-by-layer in the external electric field, which leads to an observed long-range effect. The hydrogen bonds under these conditions play possibly an auxiliary role. The value of ε° determined from the graph is equal to 3.54 kJ/mole ($a \sim 0.64$ nm^{-1}). However, this value is more likely underestimated, because, firstly, the indicated exponential relation is not accurate enough at small distances [80], and secondly, the water evaporation mechanism changes at low moisture values and relation (12) cannot be applied to determine the sorption energy.

Fig. 12 presents dependences of adsorption energy which are calculated by relation (12) and by the formula $\varepsilon_{ads} = \varepsilon^{0}\exp(-a\delta_s)$. As is seen from the Fig. 12, at small distances from the solid surface (low moisture) the exponential relation is not true. For the chosen specific surface area, this distance equals 3–4 monomolecular layers. However, it should be noted that the accepted specific surface area is of an estimated nature and was not determined for the applied wood samples experimentally.

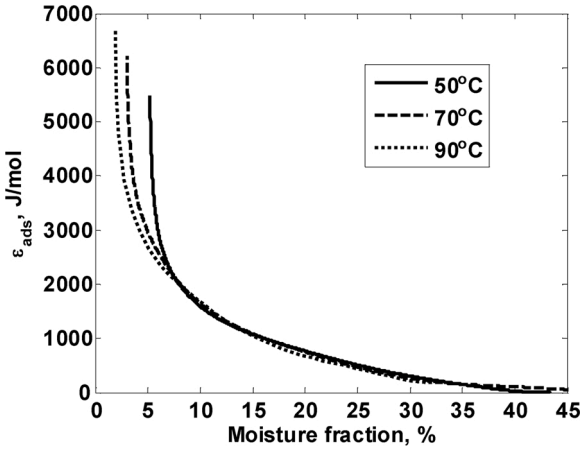

Fig. 10. Water sorption energy versus sawdust moisture fraction (w).

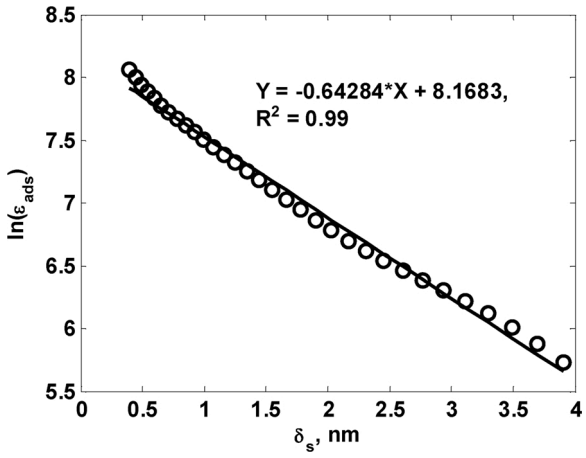

Fig. 11. Dependence of $\ln(\varepsilon_{ads})$ on δ_s for the curve of sawdust drying at 90 °C.

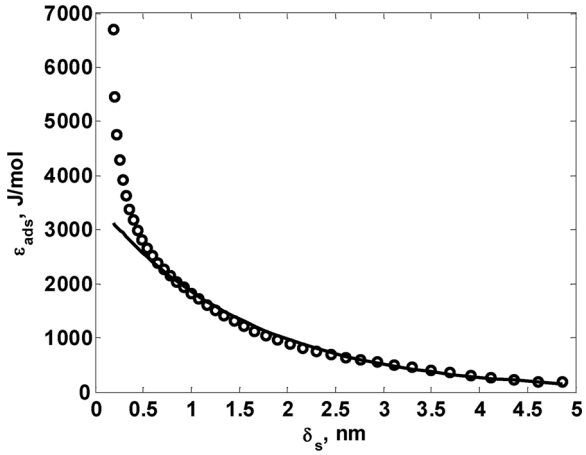

Fig. 12. Adsorption energy dependences calculated by relation (12) and by the formula $\varepsilon_{ads} = \varepsilon^{\circ}\exp(-a\delta_s)$ (solid line) for the curve of sawdust drying at 90 °C.

5. Conclusion

Study has shown the ability to use experimental data on the moisture evaporation obtained from measuring the DSC signal together with recording the thermogravimetric curve to determine the adsorption energy of moisture on the lignocellulosic raw materials surface. It should be taken into account that evaporation of liquid could significantly decrease the sample temperature compared to the detected surface temperature of the working crucible.

New method of DSC signal based correction is developed, which allows to obtain an improved estimate of actual sample temperature. Processing of experimental data on the drying of biomass, not supported by the DSC signal, can lead to significant errors in the evaluation of the thermodynamic and transport properties of the material and moisture. The estimates obtained show that the temperature of the sample during intense evaporation can be several tens of degrees below the temperature of the heating medium.

Using this temperature correction, the water adsorption energy on the surface of sawdust was measured. It is shown that such systems could be investigated using a simple experiment. In the experiment, the adsorption energy was recorded continuously as moisture evaporated, which made it possible to plot the dependence of this value on the distance to the sorption surface (thickness of the adsorbed moisture layer). The values of the adsorption energy at a pine sawdust moisture content of about 5–10 % is several kJ/mol. At lower moisture content, the adsorption energy increases sharply. According to this dependence, it is supposed that the nature of the interaction of water molecules with the sorbent surface is a long-range Coulomb force due to water dipoles orientation.

Declaration of Competing Interest

The authors declare that they have no known competing financial interests or personal relationships that could have appeared to influence the work reported in this paper.

Acknowledgements

The reported study was funded by RFBR according to the research project № 18-29-24047. The results of this study were obtained with the use of equipment of the multi-access scientific center "High-temperature circuit".

References

[1] A.V. Luikov, Theory of Drying, Energy Publ., Moscow, 1968 [in Russian].
[2] P.N. Ciesielski, M.F. Crowley, M.R. Nimlos, A.W. Sanders, G.M. Wiggins, D. Robichaud, B.S. Donohoe, T.D. Foust, Biomass particle models with realistic morphology and resolved microstructure for simulations of intraparticle transport phenomena, Energy Fuels 29 (2015) 242–254, https://doi.org/10.1021/ef502204v.
[3] W. Ai, H. Duval, F. Pierre, P. Perre, Characterization of wood micromorphology from gas permeability measurements, Microfluids Nanofluids 21 (2017), https://doi.org/10.1007/s10404-017-1936-1.
[4] J. Yin, K. Song, G. Zhao, Y. Yin, Comparison of changes in micropores and mesopores in the wood cell walls of sapwood and heartwood, Wood Sci. Technol. 49 (2015) 987–1001, https://doi.org/10.1007/s00226-015-0741-9.
[5] L. Wadso, Studies of Water Vapor Transport and Sorption in Wood. Doctoral Dissertation, Division of Building Materials, Lund University, Lund, 1993.
[6] F.J. Gomez-de la Cruz, P.J. Casanova-Pelaez, J.M. Palomar-Carnicero, F. Cruz-Peragon, Drying kinetics of olive stone: a valuable source of biomass obtained in the olive oil extraction, Energy 75 (2014) 146–152, https://doi.org/10.1016/j.energy.2014.06.085.
[7] E.T. Engelund, L.F. Thygesen, S. Svensson, C.A.S. Hill, A critical discussion of the physics of wood–water interactions, Wood Sci. Technol. 47 (2013) 141–161, https://doi.org/10.1007/s00226-012-0514-7.
[8] J. Saastamoinen, J.R. Richard, Simultaneous drying and pyrolysis of solid fuel particles, Combust. Flame 106 (1996) 288–300, https://doi.org/10.1016/0010-2180(96)00001-6.
[9] H. Thunman, K. Davidsson, B. Leckner, Separation of drying and devolatilization during conversion of solid fuels, Combust. Flame 137 (2004) 242–250.
[10] A. Galgano, C. Di Blasi, Modeling the propagation of drying and decomposition fronts in wood, Combust. Flame 139 (2004) 16–27, https://doi.org/10.1016/j.combustflame.2004.07.004.
[11] L. Burhenne, M. Damiani, T. Aicher, Effect of feedstock water content and pyrolysis temperature on the structure and reactivity of spruce wood char produced in fixed bed pyrolysis, Fuel 107 (2013) 836–847.
[12] C. Di Blasi, A. Galgano, C. Branca, M. Clemente, Analysis of the interactions between moisture evaporation and exothermic pyrolysis of hazelnut shells, Energy Fuels 30 (2016) 7878–7886, https://doi.org/10.1021/acs.energyfuels.6b00856.
[13] H. Rezaei, S. Sokhansanj, X. Bi, C.J. Lim, A. Lau, A numerical and experimental study on fast pyrolysis of single woody biomass particles, Appl. Energy 198 (2017) 320–331, https://doi.org/10.1016/j.apenergy.2016.11.032.
[14] D. Shin, S. Choi, The combustion of simulated waste particles in a fixed bed, Combust. Flame 121 (2000) 167–180.
[15] W. Zhao, Z. Li, G. Zhao, F. Zhang, Q. Zhu, Effect of air preheating and fuel moisture on combustion characteristics of corn an straw in a fixed bed, Energy Convers. Manage. 49 (2008) 3560–3565, https://doi.org/10.1016/j.enconman.2008.07.006.
[16] Y. Ding, C. Wang, X. Lu, Modeling the pyrolysis of wet wood using FireFOAM, Energy Convers. Manage. 98 (2015) 500–506, https://doi.org/10.1016/j.enconman.2015.03.106.
[17] N. Striugas, L. Vorotinskiene, R. Paulauskas, R. Navakas, A. Dziugys, L. Narbutas, Estimating the fuel moisture content to control the reciprocating grate furnace firing wet woody biomass, Energy Convers. Manage. 149 (2017) 937–949, https://doi.org/10.1016/j.enconman.2017.04.014.
[18] A. Elfasakhany, T. Klasom, X.S. Bai, Modelling of pulverised wood combustion using a functional group model, Combust. Theor. Model. 12 (2008) 883–904, https://doi.org/10.1080/13647830802094344.
[19] H. Tolvanen, T. Keipi, R. Raiko, A study on raw, torrefied, and steam-exploded wood: fine grinding, drop-tube reactor combustion tests in N2/O2 and CO2/O2 atmospheres, particle geometry analysis, and numerical kinetics modeling, Fuel 176 (2016) 153–164, https://doi.org/10.1016/j.fuel.2016.02.071.
[20] M. Jarvinen, C. Mueller, M. Hupa, C.J. Fogelholm, A CFD-applicable discrete combustion model for thermally large particles, Prog. Comput. Fluid Dyn. 11 (2011) 373–387, https://doi.org/10.1504/PCFD.2011.042847.

[21] V. Pozzobon, S. Salvador, J.J. Bezlan, M. El-Hafi, Y. Le Maoult, G. Flamant, Radiative pyrolysis of wet wood under intermediate heat flux: experiments and modelling, Fuel Proc. Technol. 128 (2014) 319–330, https://doi.org/10.1016/j.fuproc.2014.07.007.
[22] I.G. Donskoi, A.N. Kozlov, D.A. Svishchev, V.A. Shamanskii, Numerical investigation of the staged gasification of wet wood, Thermal Eng. 64 (2017) 258–264, https://doi.org/10.1134/S0040601517040024.
[23] R. Moreno, G. Antolin, A. Reyes, P. Alvarez, Drying characterisitics of forest biomass particles of Pinus radiate, Biosyst. Eng. 88 (2004) 105–115, https://doi.org/10.1016/j.biosystemseng.2004.02.005.
[24] D. Chen, Y. Zheng, X. Zhu, Determination of effective moisture diffusivity and drying kinetics for poplar sawdust by thermogravimetric analysis under isothermal condition, Bioresour. Technol. 107 (2012) 451–455, https://doi.org/10.1016/j.biortech.2011.12.032.
[25] Y. Tian, R. Wang, Thermokinetics analysis of biomass based on model-free different heating rate method, Trans. Chin. Soc. Agric. Eng. 32 (2016) 234–240. https://www.ingentaconnect.com/content/tcsae/tcsae/2016/00000032/00000003/art00034.
[26] J. Cai, R. Liu, Research on water evaporation in the process of biomass pyrolysis, Energy Fuels 21 (2007) 3695–3697, https://doi.org/10.1021/ef700442n.
[27] D.Y. Chen, D. Zhang, X.F. Zhu, Heat/mass transfer characteristics and nonisothermal drying kinetics at the first stage of biomass pyrolysis, J. Therm. Anal. Calorim. 109 (2012) 847–854, https://doi.org/10.1007/s10973-011-1790-4.
[28] A. Brys, J. Brys, E. Ostrowska-Ligeza, A. Kaleta, K. Gornicki, S. Glowacki, P. Koczon, Wood biomass characterization by DSC or FT-IR spectroscopy, J. Therm. Anal. Calorim. 126 (2016) 27–35, https://doi.org/10.1007/s10973-016-5713-2.
[29] A.V. Luikov, Heat and mass transfer in capillary-porous bodies, in: T.F. Irvine Jr., J. P. Hartnett (Eds.), Advances in Heat Transfer, Vol. 1, Academic Press, New York, 1964, pp. 123–184, https://doi.org/10.1016/S0065-2717(08)70098-4.
[30] A.V. Luikov, On the systems of differential equations for heat and mass transfer in capillary-porous bodies, Inzhenerno-Fizicheskiy Zhurnal 26 (1974) 18–25 [in Russian].
[31] A. Collignan, J.P. Nadeau, J.R. Puiggali, Description and analysis of timber drying kinetics, Drying Technol. 11 (1993) 489–506, https://doi.org/10.1080/07373939308916840.
[32] D. Martinovic, I. Horman, I. Demirdzic, Numerical and experimental analysis of a wood drying process, Wood Sci. Technol. 35 (2001) 143–156, https://doi.org/10.1007/s002260000083.
[33] R. Younsi, D. Kocaefe, Y. Kocaefe, Three-dimensional simulation of heat and moisture transfer in wood, Appl. Therm. Eng. 26 (2006) 1274–1285, https://doi.org/10.1016/j.applthermaleng.2005.10.029.
[34] D. Kocaefe, R. Younsi, S. Poncsak, Y. Kocaefe, Comparison of different models for the high-temperature heat-treatment of wood, Int. J. Therm. Sci. 46 (2007) 707–716, https://doi.org/10.1016/j.ijthermalsci.2006.09.001.
[35] A.D. Dedic, A.S. Mujundar, D.K. Voronjec, A three dimensional model for heat and mass transfer in convective wood drying, Drying Technol. 21 (2003) 1–15, https://doi.org/10.1081/DRT-120017280.
[36] S.S. Torres, W. Jomaa, J.R. Puiggali, S. Avramidis, Multiphysics modeling of vacuum drying of wood, Appl. Math. Model. 35 (2011) 5006–5016, https://doi.org/10.1016/j.apm.2011.04.011.
[37] M. Jalili, A. Anca-Couce, N. Zobel, On the uncertainty of a mathematical model for drying of a wood particle, Energy Fuels 27 (2013) 6705–6717, https://doi.org/10.1021/ef401156s.
[38] M. Simo-Tagne, R. Remond, Y. Rogaume, A. Zoulalian, B. Bonoma, Modeling of coupled heat and mass transfer during drying of tropical woods, Int. J. Therm. Sci. 109 (2016) 299–308, https://doi.org/10.1016/j.ijthermalsci.2016.06.012.
[39] M.C. Melaaen, M.G. Gronli, Modelling and simulation of moist wood drying and pyrolysis, in: A.V. Bridgwater (Ed.), Developments in Thermochemical Biomass, Springer, 1997, pp. 132–146, https://doi.org/10.1007/978-94-009-1559-6_10.
[40] C. Di Blasi, Multi-phase moisture transfer in the high-temperature drying of wood particles, Chem. Eng. Sci. 53 (1998) 353–366, https://doi.org/10.1016/S0009-2509(97)00197-8.
[41] I. Haberle, O. Skreiberg, J. Lazar, N.E.L. Haugen, Numerical models for thermochemical degradation of thermally thick woody biomass, and their application in domestic wood heating appliances and grate furnaces, Prog. Energy Comb. Sci. 63 (2017) 204–252, https://doi.org/10.1016/j.pecs.2017.07.004.
[42] T. Gabreegziabher, A.O. Oyedun, C.W. Hui, Optimum biomass drying for combustion - A modeling approach, Energy 53 (2013) 67–73, https://doi.org/10.1016/j.energy.2013.03.004.
[43] S.S. Alves, J.L. Figueiredo, A model for pyrolysis of wet wood, Chem. Eng. Sci. 44 (1989) 2861–2869, https://doi.org/10.1016/0009-2509(89)85096-1.
[44] B. Peters, C. Bruch, Drying and pyrolysis of wood particles: experiments and simulation, J. Anal. Appl. Pyrolysis 70 (2003) 233–250, https://doi.org/10.1016/S0165-2370(02)00134-1.
[45] B. Peters, H. Raupenstrauch, Modeling moving and fixed bed combustion, in: M. Lackner, F. Winter, A.K. Agarwal (Eds.), Handbook of Combustion. Vol. 4: Solid Fuels, Weinheim: Wiley-VCH Verlag GmbH& Co., 2010, pp. 257–283, https://doi.org/10.1002/9783527628148.hoc061.
[46] H. Strom, H. Thunman, A computationally efficient particle submodel for CFD-simulations of fixed-bed conversion, Appl. Energy 112 (2013) 808–817, https://doi.org/10.1016/j.apenergy.2012.12.057.
[47] H. Fatehi, X.S. Bai, A comprehensive mathematical model for biomass combustion, Combust. Sci. Technol. 186 (2014) 574–593, https://doi.org/10.1080/00102202.2014.883255.
[48] M.A. Gomez, J. Porteiro, D. Patino, J.L. Miguez, Fast-solving thermally thick model of biomass particles embedded in a CFD code for the simulation of fixed-bed burners, Energy Convers. Manage. 105 (2015) 30–44, https://doi.org/10.1016/j.enconman.2015.07.059.
[49] J.K. Gigler, W.K.P. van Loon, M.M. Vissers, G.P.A. Bot, Forced convective drying of willow chips, Biomass Bioenergy 19 (2000) 259–270.
[50] C. Di Blasi, Modeling wood gasification in a countercurrent fixed-bed reactor, Am. Inst. Chem. Eng. J. 50 (2004) 2306–2319, https://doi.org/10.1002/aic.10189.
[51] C. Mandl, I. Obernberger, F. Biedermann, Modelling of an updraft fixed-bed gasifier operated with softwood pellets, Fuel 89 (2010) 3795–3806, https://doi.org/10.1016/j.fuel.2010.07.014.
[52] A. Elfasakhany, L. Tao, B. Espenas, J. Larfeldt, X.S. Bai, Pulverised wood combustion in a vertical furnace: experimental and computational analyses, Appl. Energy 112 (2013) 454–464, https://doi.org/10.1016/j.apenergy.2013.04.051.
[53] A.H. Mahmoudi, F. Hoffmann, B. Peters, Detailed numerical modeling of pyrolysis in a heterogeneous packed bed using XDEM, J. Anal. Appl. Pyrolysis 106 (2014) 9–20, https://doi.org/10.1016/j.jaap.2013.12.001.
[54] P. Eliaers, J.R. Pati, S. Dutta, J. De Wilde, Modeling and simulation of biomass drying in vortex chambers, Chem. Eng. Sci. 123 (2015) 644–664, https://doi.org/10.1016/j.ces.2014.11.043.
[55] Nadhari WNAW, R. Hashim, M. Danish, O. Sulaiman, S. Hiziroglu, A model of drying kinetics of Acacia mangium wood at different temperatures, Drying Technol. 32 (2014) 361–370, https://doi.org/10.1080/07373937.2013.829855.
[56] C.V. Bezerra, L.H.M. de Silva, D.F. Correa, A.M.C. Rodrigues, A modeling study for moisture diffusivities and moisture transfer coefficients in drying of passion fruit peel, Int. J. Heat Mass Transf. 85 (2015) 750–755, https://doi.org/10.1016/j.ijheatmasstransfer.2015.02.027.
[57] D. Jia, X. Bi, C.J. Lim, S. Sokhansanj, A. Tsutsumi, Biomass drying in a pulsed fluidized bed without inert bed particles, Fuel 185 (2016) 270–284, https://doi.org/10.1016/j.fuel.2016.08.100.
[58] M. Madhava, P.S. Rao, T.K. Goswami, Drying kinetics of paddy using thermogravimetric analysis, Drying Technol. 19 (2001) 1201–1210, https://doi.org/10.1081/DRT-100104815.
[59] C. Di Blasi, C. Branca, S. Sparano, B. La Mantia, Drying characteristics of wood cylinders for conditions pertinent to fixed-bed countercurrent gasification, Biomass Bioenergy 25 (2003) 45–58, https://doi.org/10.1016/S0961-9534(02)00180-0.
[60] V.D. Thi, M. Khelifa, M. El Ganaoui, Y. Rogaume, Finite element modelling of the pyrolysis of wet wood subjected to fire, Fire Saf. J. 81 (2016) 85–96, https://doi.org/10.1016/j.firesaf.2016.02.001.
[61] A.H. Persad, C.A. Ward, Expressions for the evaporation and condensation coefficients in the hertz-knudsen relation, Chem. Rev. 116 (2016) 7727–7767, https://doi.org/10.1021/acs.chemrev.5b00511.
[62] H. Mounji, M. El Kouali, J. Bouzon, J.M. Vergnaud, Modelling of the drying process of wood in 3-dimensions, Drying Technol. 9 (1991) 1295–1314, https://doi.org/10.1080/07373939108916751.
[63] S.V. Syrodoy, N.Y. Gutareva, K.A. Bugaeva, Ignition of wet wood particles in the stream of high-temperature gases, MATEC Web of Conferences (2016), https://doi.org/10.1051/matecconf/20167201035, 72.
[64] J. Cai, S. Chen, Determination of drying kinetics for biomass by thermogravimetric analysis under nonisothermal condition, Drying Technol. 26 (2008) 1464–1468, https://doi.org/10.1080/07373930802412116.
[65] D. Chen, Y. Zheng, X. Zhu, In-depth investigation on the pyrolysis kinetics of raw biomass. Part I: kinetic analysis for the drying and devolatilization stages, Bioresour. Technol. 131 (2013) 40–46, https://doi.org/10.1016/j.biortech.2012.12.136.
[66] M. Bidabadi, S. Hosseinzadeh, M. Setareh, P. Panahifar, S. Sadeghi, Theoretical study of non-adiabatic counter-flow diffusion flames propagating through a volatile biomass fuel taking into account drying and vaporization processes, Fuel Proc. Technol. 179 (2018) 184–196, https://doi.org/10.1016/j.fuproc.2018.07.005.
[67] A. Elfasakhany, L. Tao, B. Espenas, J. Larfeldt, X.S. Bai, Pulverised wood combustion in a vertical furnace: experimental and computational analyses, Appl. Energy 112 (2013) 454–464, https://doi.org/10.1016/j.apenergy.2013.04.051.
[68] X. Gao, Y. Zhang, B. Li, X. Yu, Model development for biomass gasification in an entrained flow gasifier using intinsic reaction rate submodel, Energy Convers. Manag. 108 (2016) 120–131, https://doi.org/10.1016/j.enconman.2015.10.070.
[69] M.A. Gomez, J. Porteiro, D. Patino, J.L. Miguez, Fast-solving thermally thick model of biomass particles embedded in a CFD code for the simulation of fixed-bed burners, Energy Convers. Manag. 105 (2015) 30–44, https://doi.org/10.1016/j.enconman.2015.07.059.
[70] K.S. Kung, A.F. Ghoniem, Multi-scale analysis of drying thermally thick biomass for bioenergy applications, Energy 187 (2019) 115989, https://doi.org/10.1016/j.energy.2019.115989.
[71] C.V. Bezerra, L.H.M. de Silva, D.F. Correa, A.M.C. Rodrigues, A modeling study for moisture diffusivities and moisture transfer coefficients in drying of passion fruit peel, Int. J. Heat Mass Transf. 85 (2015) 750–755, https://doi.org/10.1016/j.ijheatmasstransfer.2015.02.027.
[72] R. Younsi, D. Kocaefe, Y. Kocaefe, Three-dimensional simulation of heat and moisture transfer in wood, Appl. Therm. Eng. 26 (2006) 1274–1285, https://doi.org/10.1016/j.applthermaleng.2005.10.029.
[73] S.V. Syrodoy, G.V. Kuznetsov, N.Y. Gutareva, K.A. Bugaeva, R.I. Taburchinov, The conditions and characteristics of wood particles ignition in the stream of the high temperature gases, Combust. Sci. Technol. 190 (2018) 663–686, https://doi.org/10.1080/00102202.2017.1404997.
[74] Finite element modelling of the pyrolysis of wet wood subjected to fire / V.D. Thi, M. Khelifa, M. El Ganaoui, Y. Rogaume, Fire Saf. J. 81 (2016) 85–96, https://doi.org/10.1016/j.firesaf.2016.02.001.

[75] W.J. Boettinger, U.R. Kattner, K.W. Moon, J.H. Perepezko, in: J.C. Zhao (Ed.), Methods for Phase Diagram Determination DTA and Heat-Flux DSC Measurements of Alloy Melting and Freezing, Elsevier, 2007, pp. 151–221, https://doi.org/10.1016/B978-008044629-5/50005-7.
[76] L.D. Landau, E.M. Lifshitz, Statistical Physics, Vol. 5, Elsevier, 2013.
[77] V.A. Grigoriev (Ed.), Handbook on Thermal Engineering and Technics, Energy and Atomic Publishing, Moscow, 1988 [in Russian].
[78] J.O. Hirschfelder, C.F. Curtiss, R.B. Bird, M.G. Mayer, Molecular Theory of Gases and Liquids, Wiley, New York, 1954. ISBN: 978-0-471-40065-3.
[79] A. Chesson, P.T. Gardner, T.J. Wood, Cell wall porosity and available surface area of wheat straw and wheat grain fractions, J. Sci. Food Agric. 75 (1997) 289–295.
[80] M. Plotze, P. Niemz, Porosity and pore size distribution of different wood types as determined by mercury inrtusion porosimetry, Eur. J. Wood. Prod. 69 (2011) 649–657, https://doi.org/10.1007/s00107-010-0504-0.
[81] A.W. Adamson, A.P. Gast, Physical Chemistry of Surfaces, John Wiley & Sons, New York, 1967.